



Experimental investigation on a turbulence generation system with high-blockage plates

G. Coppola, A. Gomez *

Yale Center for Combustion Studies, Department of Mechanical Engineering, Yale University, New Haven, CT 06511, USA

ARTICLE INFO

Article history:

Received 19 January 2009

Received in revised form 4 June 2009

Accepted 4 June 2009

Keywords:

Turbulence generation

High blockage

ABSTRACT

An experimental study was conducted to develop and characterize systematically a new turbulence generator system to yield large turbulent Reynolds numbers in a compact configuration. The effect of the geometric parameters of two families of high-blockage plates on the resulting turbulent flow field was systematically studied: one series of plates was characterized by the number and distribution of circular openings; a second series had non-circular opening(s) with different shapes, distribution and position of the opening(s). The plates were placed upstream of a contoured contraction and the near field at the centerline of the resulting turbulent free jet was characterized by hot-wire anemometry in terms of mean axial velocity, turbulence intensity, turbulence length scales and corresponding Reynolds numbers. The plate with a central, non-circular opening produced the best compromise of highest turbulence levels along with excellent uniformity in average velocity and turbulence intensity, as evidenced by scan in the transverse direction. It appears to be the most promising one. By comparison with more traditional approaches to turbulence generation, we increased the turbulent Reynolds numbers based on the integral length scale to values on the order of 1000, which was one of the design objectives. Other plate geometries also yielded intense turbulence, but, in some cases, exhibited spurious frequency peaks in their power spectrum. The turbulent generation approach is to be adapted to combustion studies to reproduce conditions typical of practical system in relatively small experimental set-ups that are well-suited for bench-top experiments.

© 2009 Elsevier Inc. All rights reserved.

1. Introduction

To mimic the behavior of practical systems in a laboratory set-up typically requires the establishment of highly turbulent flows in relatively confined systems and at flow rates much smaller than in applications. Cost considerations and experimental limitations may in fact prevent the duplication of a practical system both in terms of size and flow rates. Case in point are reacting flows of gas turbines for which scaling considerations suggest operating in a certain regime of turbulent Reynolds number, $Re_l = u'l/\nu$, where l is a suitable turbulent length scale, u' the turbulence intensity and ν the kinematic viscosity. That a turbulent Reynolds number, based on either an integral scale, L , or a Taylor scale, λ , rather than an engineering Reynolds number based on a macroscopic scale such as an outlet diameter and an average velocity, Re_D , ought to be the critical scaling parameter is self evident from a turbulence viewpoint, since Re_l defines the range of length and time scales of the problem. If such a range is sufficiently broad, as is the case for sufficiently large Re_l , the flow has the necessary prerequisites

of “true” turbulence and the study may have some general value. Since in the first approximation flow rates define the engineering Re_D , the task is often to maximize Re_l for a given Re_D by using suitable turbulence generation schemes, and yet preserve reasonably well behaved velocity profiles. This is the objective of the present investigation with the ultimate goal of applying the most promising approach to combustion applications in well-controlled and compact systems.

To generate turbulence in wind tunnels [1] and in axisymmetric tubes [2], we can distinguish between two approaches: passive ones, involving high velocity streams and jets issuing into a mainstream; and active ones involving, for example, oscillating grids. Both turbulence generation schemes show similar relative intensities, at ~20%, but with very different streamwise locations where the flow shows good symmetry/uniformity characteristics: ~130 jet diameters for the passive, jet approach and ~1 jet diameter for the active one, respectively. Passive grids are typically limited to more modest turbulence intensities ~10%. For example, with a measured integral scale, L , on the order of 0.5 mm for every flow condition [2], Re_l ranging from 100 to 223 were achieved for the passive approach and from 144 to 288 for the active one, at main-stream velocities of 27 and 39 m/s, respectively. The mixing layer downstream of a free jet with its high levels of relative turbulence

* Corresponding author. Tel.: +1 203 432437; fax: +1 203 4327654.

E-mail addresses: gianfilippo.coppola@yale.edu (G. Coppola), alessandro.gomez@yale.edu (A. Gomez).

Nomenclature

D_{out}	inner diameter of nozzle outlet	u'	root mean square axial velocity
H	plate distance from nozzle exit	L	integral length scale
R_s	radial position of the plate openings	λ	Taylor length scale
R_p	plate radius, based on $\frac{1}{2}$ of the wetted diameter	$\bar{\epsilon}$	mean energy dissipation rate
d	characteristic dimension of the plate opening(s)	Re_D	engineering Reynolds number based on D_{out} and U_{out}
N	number of openings on a plate	Re_L	Reynolds number based on the integral length scale, L , and u'
A_e	plate open area	Re_λ	Reynolds number based on the Taylor length scale, λ , and u'
A_p	plate area	Re_d	Reynolds number based on the characteristic length scale, d , of the plate opening
ν	gas kinematic viscosity		
U	mean axial velocity		
U_{out}	mass average axial velocity at nozzle exit section		

intensity has been exploited as turbulence generator [3] to study the effect of high turbulence levels, for example, on heat transfer and combustion [4]. More recently, fractal wakes generators [5] and fractal grids [6] have been exploited for multi-scale energy injection with the same purpose, with a focus on the effect of the fractal dimension and of different geometrical parameters on the turbulence characteristics of the flow.

From a combustion perspective, reasonable turbulence levels are typically generated in high-speed reactant jets. Flame extinction/blow off limits the turbulence levels achievable, by limiting the maximum jet velocity. Different solutions have been adopted to overcome this limit, ranging from pilot flames [4] to bluff body [7] or swirl stabilization [8], each introducing new challenges, especially for computational modelers of those flames. A potentially “clean” alternative that has found some limited success relies on aerodynamic stabilization. It entails mounting two jets opposite to each other and anchoring the flame in the resulting stagnation flow field without resorting to any pilot. Grid or plate turbulence generators are adopted to boost the turbulence levels and the most common approach is to use a perforated plate *downstream* of a contracting nozzle. This approach allowed Kostiuk et al. [9] to achieve $\sim 12\%$ of relative turbulence intensity, an integral scale $L \sim 2.25$ mm and $Re_L = 165$, based on such a scale, as measured close to the jet exit. Even more modest values were reported by Kitajima et al. [10] ($Re_L \sim 50$ with relative intensities up to $\sim 8\%$). Yoshida et al. [11] designed a turbulence generator, which consisted of 18×4 closed-end tubes, each of which had four 1.5 mm holes equally spaced around it. The jets impinge on each other and produce a turbulent $Re_L \sim 220$. In another study [12] the same authors developed yet another design specifically to study counterflow premixed and diffusion flames relying on the turbulence generation by opposed jets. The group in Darmstadt has performed some of the most comprehensive investigation to date on these types of flames [13–16]. But also in their case, the turbulent Reynolds numbers tend to be low, on the order of 100.

Clearly in all of these studies, the turbulence is weak, which makes these experiments less relevant to practical applications. Possibly, this is the reason why counterflow turbulent flames have not been embraced by the combustion community, despite the enormous success of its laminar counterpart that is the prototypical well-defined combustion environment [17]. Yet, the advantage of pilotless flame stabilization is very significant if these flames are to be computationally modeled without *ad hoc* assumptions. The modeling of pilot flames, with attending burner losses that are difficult to quantify, and their influence on the turbulence, pose notorious computational challenges. Our ultimate objective is to contribute to the counterflow turbulent combustion literature by circumventing the above mentioned Re_L limitations.

Clearly, to establish strong turbulence we cannot let it develop from shear flows by impinging jets hundreds of diameters apart. In

a typical counterflow configuration the nozzles are about one or two diameters apart, to reduce interference of the ambient air or inert shroud on the gas composition and ensure stable flames. As a result, we are left with the challenge to develop highly turbulent and reasonably homogeneous flows *inside* the nozzle. Most interesting in this context is an approach that was inspired by some internal combustion engine applications using either a 2D [18] or an axisymmetric [19] slot, *upstream* of a converging nozzle unlike [9,10] to generate vigorous turbulence intensities, up to 40%, and Re_L up to 1600. Of all the available turbulence generation schemes, these designs seem to be able to produce the most intense turbulent fields, at the cost of lack of homogeneity and isotropy. These authors did not examine systematically the effect of geometrical parameters on the turbulence characteristics of the flow.

The aim of the present work is to develop and characterize systematically a new turbulence generator scheme suited to study non-premixed and premixed flames under intense turbulence, yielding $Re_L = O(1000)$. We investigated a variety of high-blockage plates, partly inspired by previous designs [18,19], and the influence of many geometric parameters. In view of the large number of plates and the extensive parameter space to be explored, single-point data at the center of the nozzle exit section were collected first to classify the plates. Subsequently, radial scans are used to assess the radial uniformity for the most promising configurations.

2. Experimental system

2.1. Experimental set-up

The plates were tested in the nozzle assembly shown in Fig. 1. N_2 gas entered at the bottom and went through a flow conditioning section, consisting of two honeycombs measuring ~ 46.6 mm in diameter, 38 mm apart from each other. Each honeycomb was 19 mm thick with a 0.8 mm cell size. The uniform flow leaving the conditioning section was then forced through a perforated/slotted plate (Fig. 2), positioned at a variable distance, H , from the nozzle exit section. Depending on the radial position of the plate opening(s), R_s , the flow would impact the top surface of the nozzle. It eventually exited through the 12.7 mm diameter opening at the nozzle top (Fig. 1b). The flow rate was controlled by digital flow controllers (Teledyne-Hastings 300D series) providing readout and full scale accuracies of $\pm 0.5\%$ and $\pm 0.2\%$, respectively. The estimated uncertainties at the minimum (30 slpm) and maximum (90 slpm) flow rate were $\pm 2.50\%$ and $\pm 1.20\%$, respectively.

Turbulence characteristics were derived from velocity measurements by hot-wire anemometry. A high frequency (up to 150 kHz) response anemometer (IFA 100, TSI Inc.) was used and a single sensor probe (TSI, Inc., Model 1212) made of a 5 μm diameter (d_w) sil-

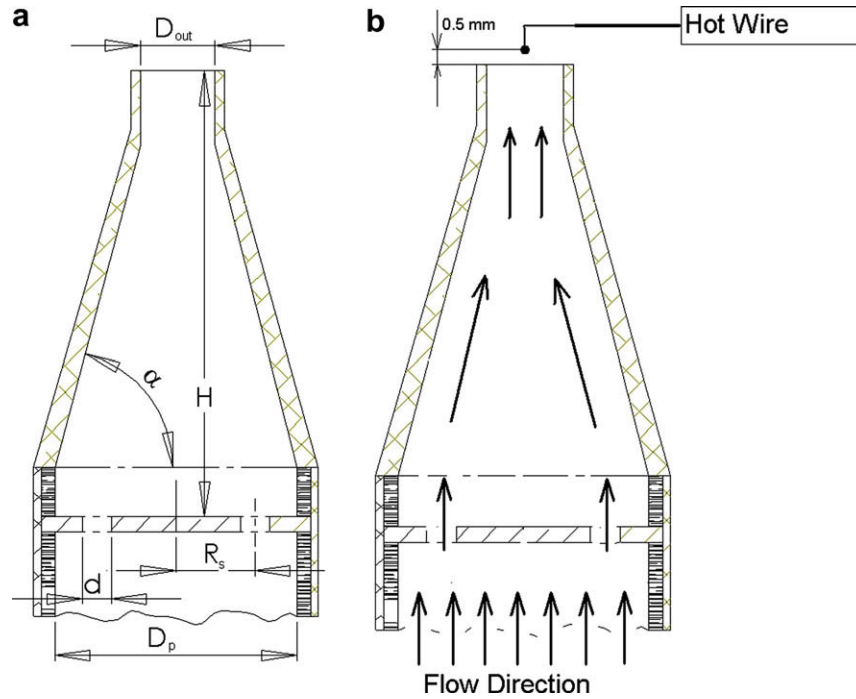


Fig. 1. (a) Schematic drawing of the plate-nozzle assembly: H is the axial distance of the plate from the nozzle exit section; D_{out} is the nozzle outlet diameter; α is the nozzle contraction angle; R_s is the radial position of the opening center; d is the plate opening diameter; D_p is the plate wetted diameter in the section upstream of the contraction; (b) Schematic drawing of the mean flow pattern through the nozzle with the hot-wire probe in position.

ver coated platinum wire with a 1.27 mm sensitive length (l_w), resulting in an $l_w/d_w \sim 250$. The hot wire was calibrated using a unit (TSI, Inc., Model 1125) consisting of a contoured nozzle, producing a very flat and laminar flow at the exit section, a pressure transducer, allowing for a very accurate measurement of the flow rate, and a probe holder, to position the sensitive wire at the center of the nozzle exit section and perpendicular to the flow. During each calibration, performed under the highest flow rate conditions, a square wave test was performed to guarantee a stable and fast wire response.

2.2. Data analysis and uncertainty estimates

All the data were sampled at the maximum sampling frequency allowed by the data acquisition board $f_s = 200$ kHz and high-pass filtered at $f_a = f_s/2 = 100$ kHz to prevent aliasing. The length of each record was chosen to be the largest allowed by the system memory capability, which resulted in records of up to $8.4 \cdot 10^6$ points ($\sim 65,000$ integral time scales). The one-dimensional power spectrum in the frequency space, E_1 [20], was estimated by the Welch method [21], by which after dividing the record in many sub-records (typically ~ 1000) with 50% overlap, the power spectrum was estimated on each sub-record by applying a Hamming window [21], and averaging was performed on all sub-records. The integral length scale, L , was estimated by fitting the estimated power spectrum with the von Karman's turbulent spectrum [22]

$$\frac{UE_1\{f\}}{Lu^2} = 4 \left[1 + \left(\frac{8\pi fL}{3U} \right)^2 \right]^{-5/6}, \quad (1)$$

where f is the frequency, u'^2 is the velocity variance and U is the mean velocity. The transverse Taylor length scale, λ , was estimated from the mean energy dissipation rate, $\bar{\varepsilon}$, according to the equation

$$\lambda = \left(\frac{15\nu u'^2}{\bar{\varepsilon}} \right)^{1/2}, \quad (2)$$

where ν is the kinematic viscosity [23]. The mean energy dissipation rate, $\bar{\varepsilon}$, was estimated by fitting the power spectrum inertial subrange to the equation [23]

$$E_1\{k_1\} = \frac{18}{55} A \bar{\varepsilon}^{2/3} k_1^{-5/3}, \quad (3)$$

where $k_1 = 2\pi f/U$ is the wavenumber and $A = 1.62$ is a constant [22]. The statistical uncertainty was estimated by assuming a general distribution for the samples [24] and 95% confidence. The error propagation rules were applied to estimate the uncertainties in the derived quantities. Conservatively, we assumed a $\pm 3\%$ uncertainty for a single velocity sample related to the apparatus, including calibrator [25]. The errors resulting from high turbulence intensity were also taken into account and estimated from [26]. The resulting total uncertainty comprises the flow metering system uncertainty, the measurement system uncertainty for a single sample, the statistical uncertainty and the uncertainty arising from the turbulence levels effect on the hot wire.

2.3. Turbulence generators

All plates were built by laser cutting a 2.54 mm thick cast acrylic plate with outer radius $R_p = 23.18$ mm. The laser cutting system (Universal Laser Systems Inc., Model V-35) had an accuracy of $\pm 0.01667\%$ and a beam diameter at the focal point of 0.127 mm, which limited the size of smallest feature/hole. Two families of turbulence generators were considered: Multi-circular jet plates (MCJ) and non-circular jet plates (NCJ). The MCJ series (Fig. 2, top left) had a number of holes positioned at equal intervals in the azimuthal direction and at a fixed radial position. The plates in this series are geometrically defined by the hole diameter, d , the number of holes N and their radial position R_s . The open area of this type of perforated plate is given by $A_e = NA_h$, where A_h is the area of a single hole of diameter d .

To explore the possibility of affecting turbulent scales and flow homogeneity with a more complex plate design, we considered also

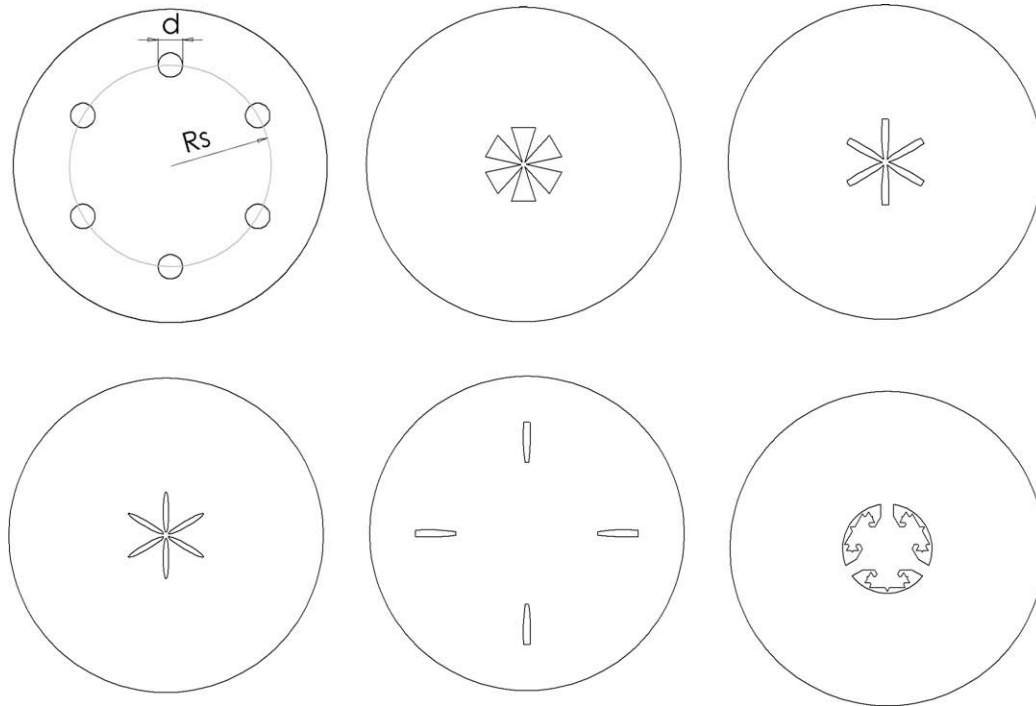


Fig. 2. Turbulence generator families: multi-circular jet (MCJ) plate (top left) and non-circular jet (NCJ) plates (single-jet (top center); central-jet (top right); central wake (bottom left), multi-jet (bottom center), wake (bottom right)).

the flow through openings of different non-circular shapes. Many examples of flows from non-circular geometries have been reported, showing different features, like streamwise vortices, higher instability, tendency to symmetry, etc. We considered a non-circular geometry as a good candidate for turbulence generation in a system like the one under investigation and explored different geometric (sharp corners, lobed orifices and fractal openings) and flow configurations (jets and wakes), to exploit their flow features. The resulting geometries have been classified according to the plate dominant geometric arrangement into four different sub-families: single-jet (SJ), central-jet (CJ), central wake (CW), wake (W), multi-jet (MJ). For brevity, only one plate representative of each family is presented. The single-jet (Fig. 2, top center) is the simplest one, as it consists of a hole at the plate center with different types of protrusions (triangular in the present design). The central-jet (Fig. 2, top right) is the evolution of the single-jet, where the protrusions area becomes larger than the open area, and the shape resembles multiple slit openings in a radial pattern connected at the center. The central wake (Fig. 2, bottom left) is a variant of the central-jet, where the protrusions meet at the center of the plate, blocking it and the result is a plate with a number of disconnected openings close to the plate center in a radial pattern. The multi-jet (Fig. 2, bottom center) implies multiple opening of the same type positioned at equal intervals and at the same radial position, as in the previous series. The wake (Fig. 2, bottom right) can be generated by partially blocking the opening of a plate or placing an object downstream of the plate generated jets. In this case, each jet will generate a wake that, depending on the holes radial position, may impact the nozzle wall, stretch/break the wake related structures and emerge from the nozzle exit section. In all cases, the plate outer radius measured $R_p = D_p/2 = 23.18$ mm.

We also considered two additional families of plates, one with a circular slot and the other with a single circular opening in the center. For brevity we are not presenting results on these series because they were less promising as compared to the two series discussed below.

3. Results and discussion

To cover as wide a parameter space as possible, a first screening of the turbulence generators was based on single-point measurements on the centerline, ~ 0.5 mm above the nozzle exit (Fig. 1b). In selected cases, radial scans were performed to check for radial uniformity and correlate it with the single-point measurements. Indeed, the normalized mean centerline axial velocity is a reasonably good predictor of uniformity of the mean velocity profile along the radial direction for symmetric patterns. Results are presented in terms of: mean centerline axial velocity, U , normalized by the mass average velocity at the plate at the specific flow rate, U_{out} ; turbulence intensity, u' , normalized by the mean centerline velocity, U ; turbulent longitudinal integral scale, L ; Taylor microscale, λ , both normalized by the nozzle diameter, and the turbulent Reynolds numbers based on these scales, Re_L and Re_λ , respectively. The rationale for this selection is that we wish to maximize the ratio of turbulent Reynolds number(s) to the engineering Reynolds number, Re_D , without compromising the uniformity of the flow in the radial direction. For example, $Re_L/Re_{Dout} = (L/D_{out})(u'/U)(U/U_{out})$, with the three non-dimensional variables to be shown in subsequent figures. This goal is achievable by maximizing L/D_{out} and u'/U and keeping U/U_{out} as close to unity as possible for the radial uniformity constraint.

The contoured nozzle and the large contraction ratio used in this work, reduce possible flow asymmetry, producing profiles that could be assumed symmetric for the purpose of this work. In view of the large number of plates investigated, radial profiles were measured only for the most interesting plates. At fixed flow rate, the plate open area, A_e , is expected to play a central role in the plate performance, since it affects the energy injection at the large scales. Because of the high blockage used, this parameter is expressed in relative terms, as the percentage of plate open area with respect to the plate total area, $\%A_e = 100 A_e/A_p$, where $A_p = \pi R_p^2$ is the plate total area and R_p is the plate wetted radius. The holes/slot radial position is normalized by the nozzle exit section radius, R_{out} ,

and the non-dimensional quantity $R' = R_s/R_{out}$ will be used throughout the discussion. The distance, H , between each plate and the nozzle exit section is normalized by the plate wet diameter, D_p , or nozzle base inner diameter. Also use will be made of the plate Reynolds number defined as $Re_p = U_p d/\nu$, where d is the hole/opening characteristic length and U_p is the hole mass averaged velocity.

3.1. Turbulence characteristics multi-circular jet plates (MCJ Series)

The multi-circular jet plates (MCJ Series) (Fig. 2, top left) were designed to understand the effect, if any, of the non-dimensional radial position of the holes, R' , their number, N , and the plate open area ratio, $\%A_e$. The normalized mean centerline velocity shows a tendency to increase with Re_p (Fig. 3, top left). At fixed flow rate, an increase in Re_p is achieved by decreasing d and/or N , and at every radial position, N can be considered an indirect inverse measure of the jet-to-jet distance. Increasing this distance, or decreasing N (Fig. 3, top right) increases U/U_{out} , probably by delaying the jet-to-jet momentum exchange, producing a flow less and less uniform. On the other hand, fixing N , and increasing d , increases the $\%A_e$, which, in turn, lowers the jet exit velocity at the plate and consequently the U/U_{out} ratio, thereby producing more uniform mean profiles at the nozzle exit section. The holes radial position, R' , also influences the U/U_{out} ratio, although through a seemingly non-monotonic behavior (Fig. 3, bottom left). In fact, the U/U_{out} ratio seem to decrease from small ($R' < 1$) to about $R' \sim 1$ and possibly increase again at larger R' . The radial position also affects the jet-to-jet distance, therefore we would expect it to produce an effect similar to N , which seems to be the case for $R' > 1$. In reality the flow pattern in the nozzle is quite different depending on whether $R' < 1$ or $R' > 1$. In fact, for $R' < 1$ the jets are directly under the nozzle exit section, and should behave more like a free jet, while for $R' > 1$ the jets impact onto the nozzle wall and develop into a wall

jet, before leaving the nozzle. Increasing the non-dimensional distance, H/D_p , between the perforated plate and the nozzle exit section (Fig. 3, bottom right) has the expected effect of lowering the U/U_{out} ratio, resulting in more uniform mean velocity profiles. The larger distance, in fact, allows the jet to develop and merge by the time they reach the nozzle exit section and the flow has adjusted to the local geometric configuration. For $R' < 1$ (not shown) the turbulent jets spread with an angle of $\sim 20^\circ$ and merge at a distance of about $3 \times$ their separation [27], while for $R' > 1$ the jets may or may not merge before impacting onto the nozzle inner wall, depending on the ratio between the merging distance and the jet to wall distance. In any case, the wall jet emerging after the impact will merge faster, having a spreading rate about $3 \times$ higher than in free jets [28].

The radial scans of the normalized mean velocity (Fig. 4) confirm the trends observed by evaluating the U/U_{out} ratio, showing a more pronounced bell shape profile with small N and at large R' . It should be noticed that some plates show some degree of asymmetry in the profiles, which can be the result of a large scale instability induced by the high blockage [27] and are possibly triggered by small geometric imperfections. The mechanism of such instabilities has been investigated by others [27,29–31] and is beyond the scope of this work.

The turbulence relative intensity increases linearly with Re_p (Fig. 5, top left) to a good approximation. Notice the large values achieved with the present plate. Decreasing the $\%A_e$ increases the mean velocity at the plate, which results in higher turbulence levels, while the mean velocity at the nozzle can change only to a limited extent and is locked by the flow rate. At fixed $\%A_e$, and flow rate, increasing Re_p requires increasing d and appropriately decreasing N , which again has the effect of boosting the fluctuations (Fig. 5, top right). The holes radial position, R' , has a strong influence on the turbulence intensity (Fig. 5, bottom left), which decreases with increasing R' , to reach what could be a plateau for

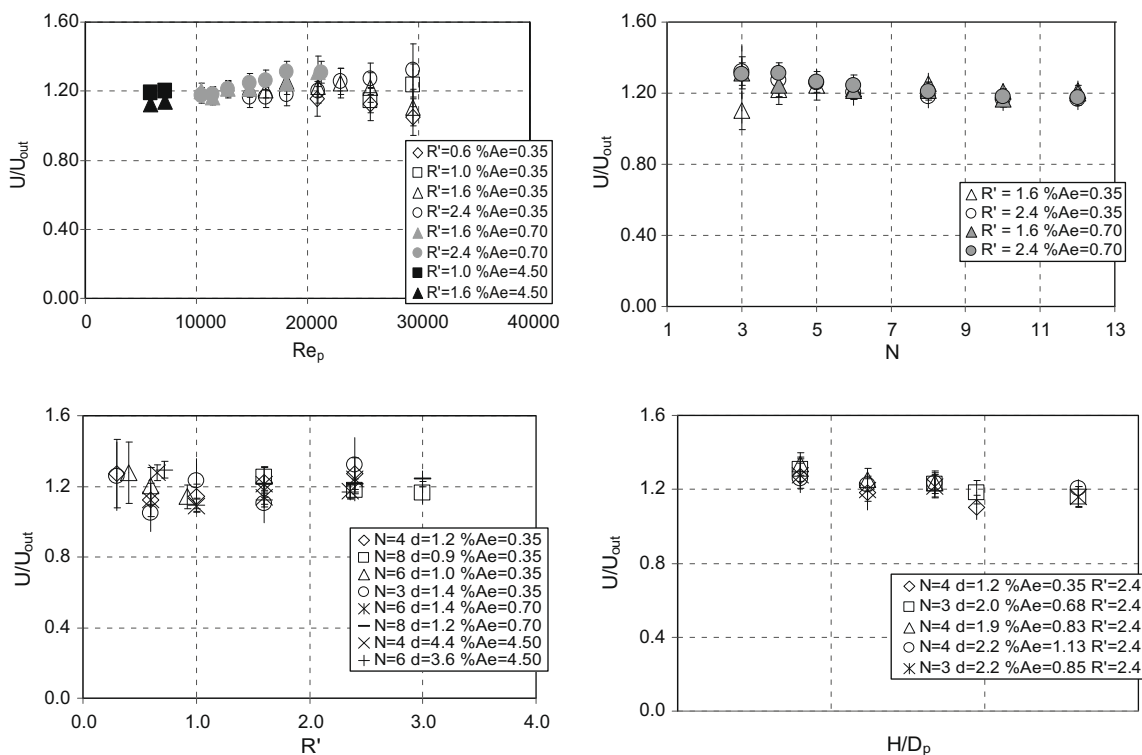


Fig. 3. Normalized centerline velocity of multiple circular jet plates (MCJ Series) at $Re_D \sim 10000$ and fixed $H/D_p \sim 1.4$, as a function of: Re_p (top left) and N (top right), both parametric in R' and $\%A_e$; R' (bottom left) and H/D_p (bottom right), both parametric in N and $\%A_e$.

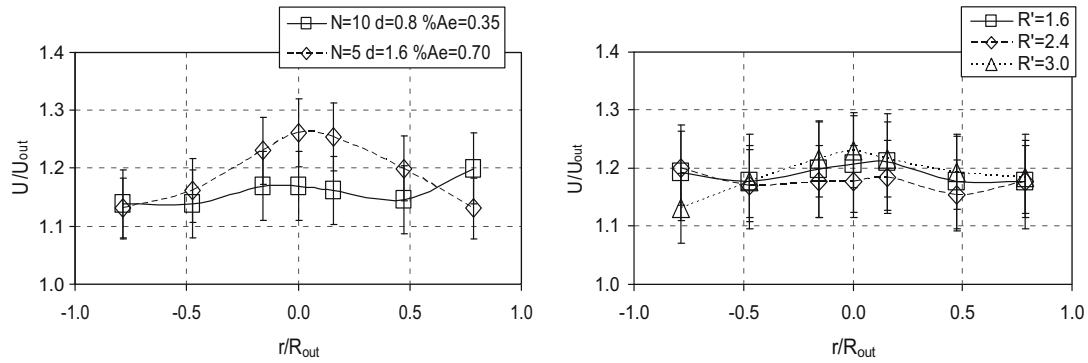


Fig. 4. MCJ Series radial profiles of the mean axial velocity component scaled by the mean centerline velocity, at $Re_D \sim 10,000$ and $H/D_p \sim 1.4$. Left: radial profile parametric in N and $\%A_e$. Right: radial profile parametric in R' .

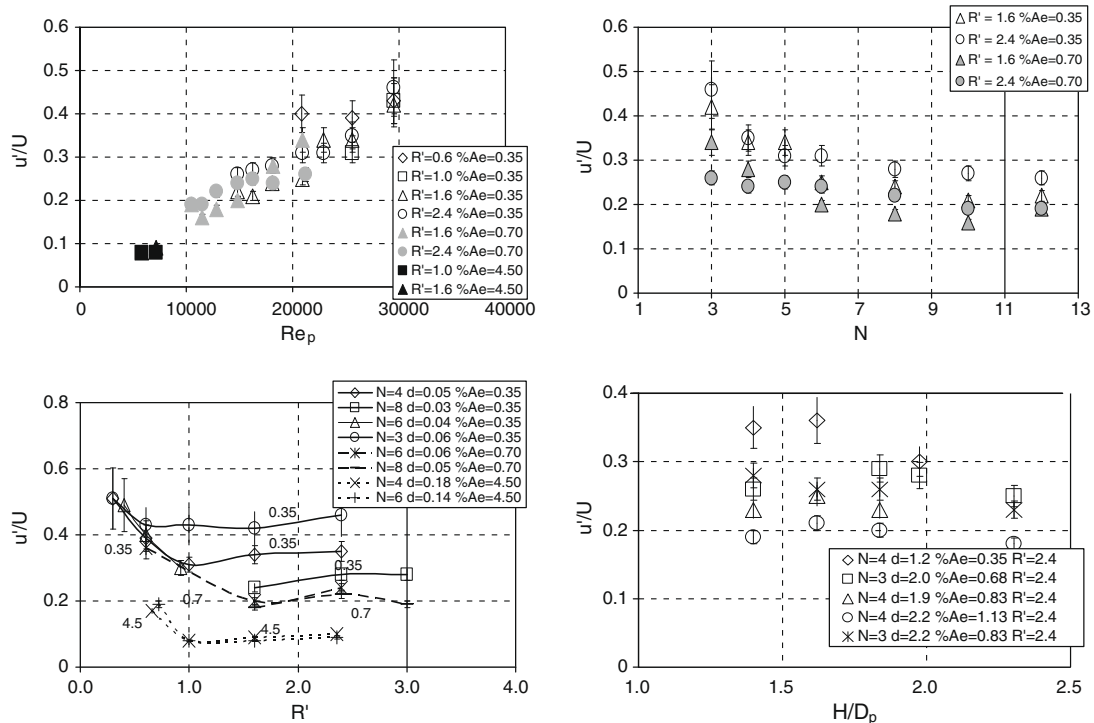


Fig. 5. Axial rms velocity normalized by the local mean value for multiple circular jet plates (MCJ Series) at $Re_D \sim 10,000$ and fixed $H/D_p \sim 1.4$, as a function of: Re_p (top left), and N (top right), both parametric in R' and $\%A_e$; R' (bottom left) and H/D_p (bottom right), both parametric in N and $\%A_e$.

$R' > 1$, suggesting the existence of two regimes. In fact, for $R' < 1$ the jets emerge from the plate, possibly merge and reach the nozzle exit section, behaving, overall, as free jets; for $R' > 1$ the jets emerge from the plate, and impact the nozzle wall, forming wall jets, before reaching the nozzle exit section. The different behavior at $\%A_e = 0.35$ can be explained as a Re_p or N effect. In the first case, we notice that at fixed $\%A_e$ and flow rate, Re_p increases linearly with d , explaining the increase of the turbulence intensity with d . On the other hand, the fluctuations increase with decreasing number of holes. In the absence of flow visualization because of lack of optical access, one can speculate that the jet-to-jet interaction may be playing a role by inducing instabilities [27] in the flow and these instabilities may be favored by the larger separation between the jets and high velocity. At $\%A_e > 0.35$ this effect seems to be negligible, probably supporting the idea of an instability based on jet-to-jet interaction, with a critical value for Re_p . Moving the plate further away from the nozzle exit section has the effect of decreasing the turbulence intensity, and there seem to be a critical

value of the distance before the decrease becomes evident at $\sim 1.8D_p$. This suggests that the rate of decay is regulated by the nozzle geometry (its internal diameter) and not by the plate hole diameter. Significantly, the plates achieve a good radial uniformity in turbulence intensity (Fig. 6), which seem to slightly deteriorate with increasing R' .

The integral scale is relatively unaffected by Re_p and N (Fig. 7, top), falling for most part in a band between $0.29D_{out}$ and $0.34D_{out}$, corresponding to 3.75 and 4.25 mm, respectively. The exception are the plates with the largest area ratio (and lowest Re_p), with values of about $0.15D_{out}$. The holes radial position (Fig. 7, bottom left) also has a weak influence, while the plates with $\%A_e \sim 4.5$ show a large variation with the radial position, with values falling to about $0.15D_{out}$ for $R' > 1$, suggesting the existence of a Re_p -dependent transition in the large scale dynamics. The integral scale grows with H/D_p (Fig. 7, bottom right), independently of Re_p , with a possible asymptotic value of $\sim 0.35D_{out}$. Overall, the values of the integral scale, for $Re_p > 10,000$, fall within the range $0.3D_{out} - 0.35D_{out}$. If

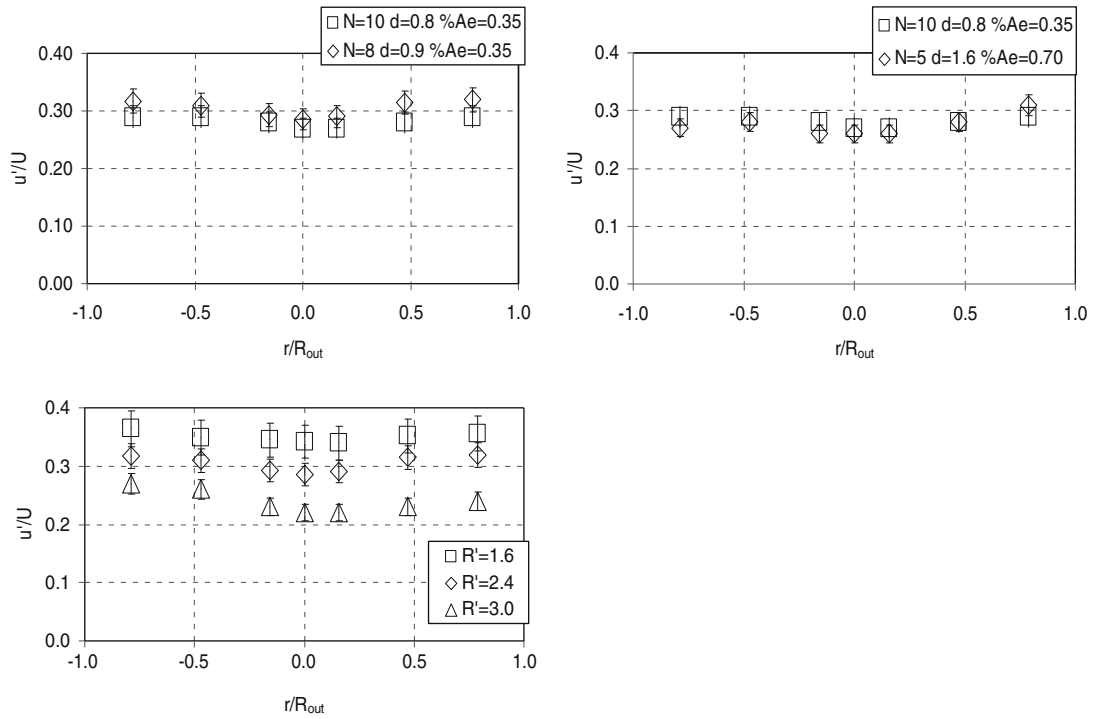


Fig. 6. MCJ Series radial profiles of the axial velocity rms normalized by the local mean axial velocity, at $Re_D \sim 10,000$ and $H/D_p \sim 1.4$. Top left: radial profile parametric in N and $\%A_e$. Top right: radial profile parametric in $\%A_e$. Bottom: radial profile parametric in R' .

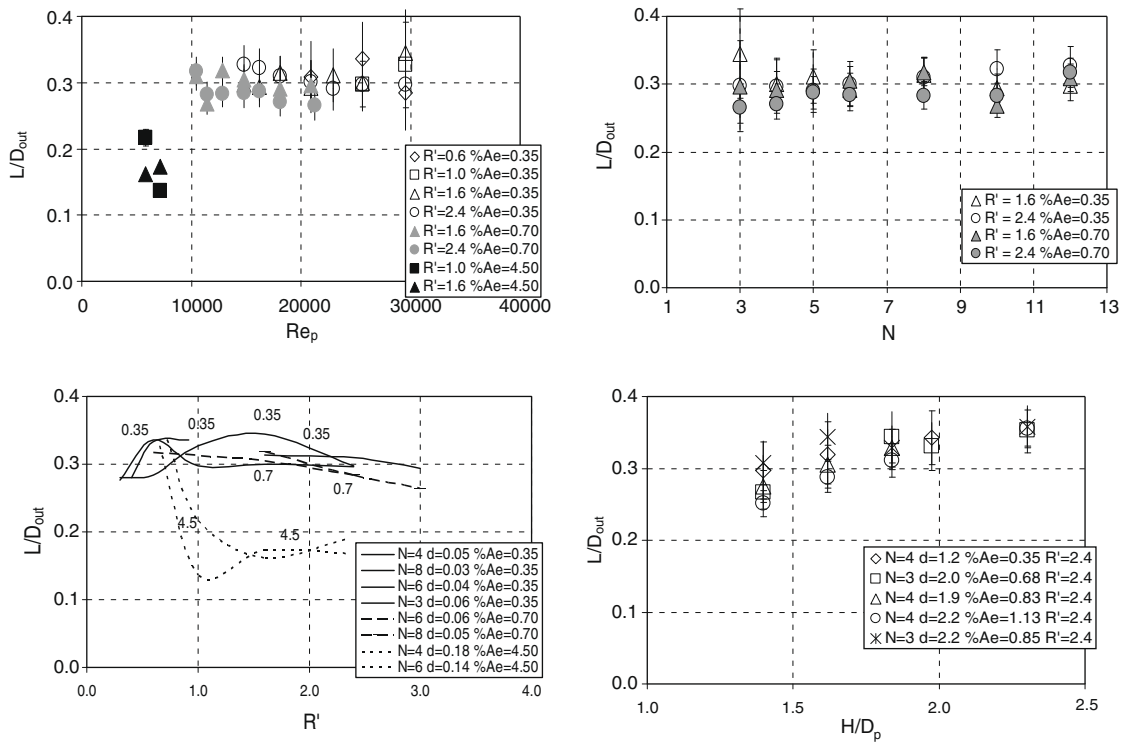


Fig. 7. Normalized integral length scale of multiple circular jet plates (MCJ Series) at $Re_D \sim 10,000$ and fixed $H/D_p \sim 1.4$, as a function of: Re_p (top left), and N (top right), parametric in R' and $\%A_e$; R' (bottom left) and H/D_p (bottom right), parametric in N and $\%A_e$.

we normalize the integral scale by the plate wet diameter, D_p , the range becomes $0.075D_p - 0.097D_p$, which is in reasonable agreement with the existing literature [32] on confined single-jets, in spite of the different geometry. This last observation may suggest that the integral scale is locked by the nozzle base internal diame-

ter (or plate wet diameter) [32–34] rather than by the plate hole diameter [35].

The Taylor scale decreases with increasing Re_p and N (Fig. 8, top) independently of R' and $\%A_e$. The dependence on R' (Fig. 8, bottom left) is not simple, but overall λ seems to increase as the holes

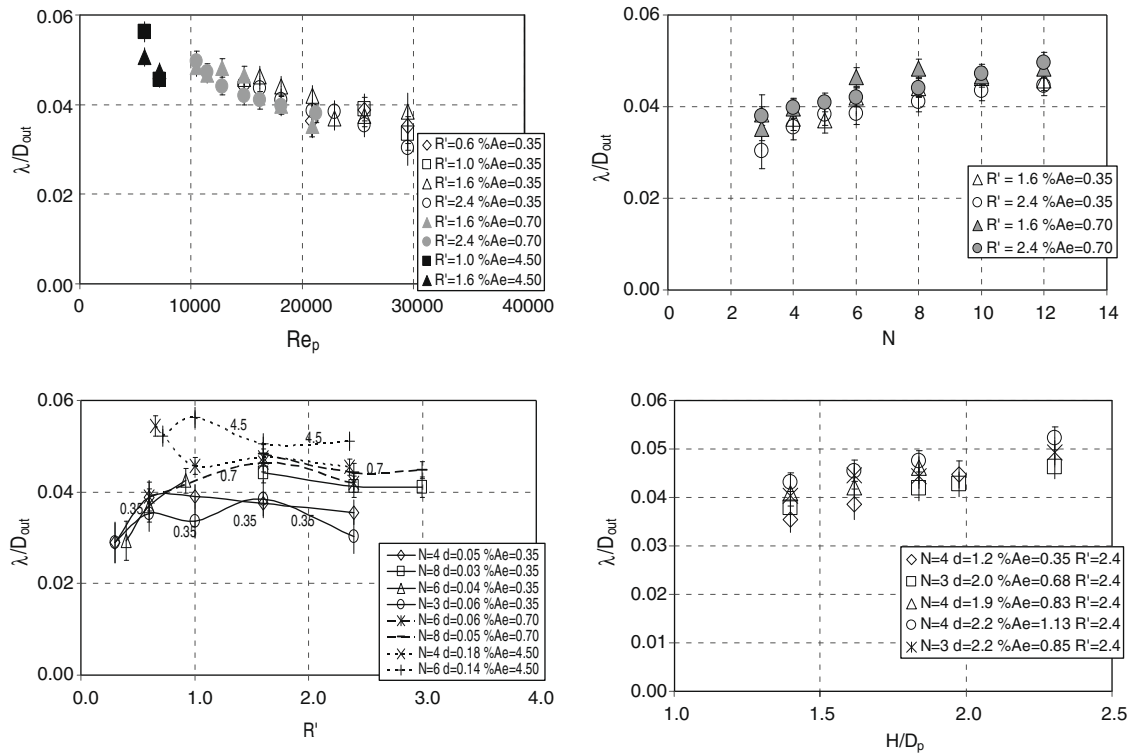


Fig. 8. Normalized Taylor length scale of multiple circular jet plates (MCJ Series) at $Re_D \sim 10,000$ and fixed $H/D_p \sim 1.4$, as a function of: Re_p (top left), and N (top right), parametric in R' and Ae_c ; R' (bottom left) and H/D_p (bottom right), parametric in N and Ae_c .

are positioned farther and farther away from the center of the plate. Increasing the distance of the plate from the nozzle exit section (Fig. 8, bottom right), has the effect of increasing λ , independently of the area ratio. The turbulent Reynolds numbers, based on the integral and the Taylor length scales, follow quite closely the trends observed for the relative intensity with respect to R' and H (Fig. 9), with values on the order of 2000 and 200, respectively for the centermost positions and small area ratios. Notice that the objective of achieving a healthy turbulence has been achieved under the present conditions. On the other hand, values on the order of 150 and 60 for Re_L and Re_c are obtained for $R' > 1$ and high area ratios. The Reynolds numbers dependence on H also suggests the existence of an optimal position, dependent possibly on the hole diameter.

We analyzed the shape of the power spectrum of the flow generated by the plates and noticed for some of the plates a small ‘bump’ at a frequency, $f \sim 650$ Hz, as shown in Fig. 10. At the highest plate average velocity, this ‘bump’ becomes more noticeable as the jets radial position $R' \rightarrow 0$, with a possible critical value at $R' = 2.4$. As the plate average velocity decreases, so does the critical value, and for the peak to become noticeable the radial position, R' has to be 1 or less. Decreasing N or increasing Re_p (Fig. 10, left) has a damping effect on the peak, as it gets less pronounced till it disappears completely for $N = 3$. Larger radial position or lower number of jets imply a larger distance between the jets, suggesting that the peak could be induced by jet-to-jet interaction. Although not shown here for brevity, flow rate has no influence on the peak frequency therefore Re_p does not seem to be playing a role. Although we can only speculate on the origin of the ‘bump’, we did observe that this feature is present only for some plates and as such it can be avoided by properly choosing the geometric parameters. Since the extent of the inertial range in the power spectrum is on the order of one decade, the system does not appear to be well-suited to study scaling laws generally requiring a much broader inertial range.

In summary, the multi circular jet plate configuration offers a reasonably good control over the relative fluctuations, length scales and turbulent Reynolds numbers. The plates seem to operate under three regimes, depending on holes radial position, R' and Re_p . The insurgence of a peak in the spectrum and of mean flow asymmetry under some conditions does, however, reduce the range of achievable turbulent Reynolds numbers. Homogeneity is relatively good and is affected by R' and N , improving by increasing N or decreasing R' . The turbulent Reynolds’ numbers are directly proportional to the plate Reynolds number. If the objective of inserting such a plate is to induce the largest possible turbulent Reynolds’ numbers at a given flow rate without sacrificing radial homogeneity in the velocity profiles, the present data suggests that the highest turbulence levels are achieved for small open area, small N and $R' < 1$. Also, the plate should be close to the nozzle exit section, if one can tolerate less homogeneous mean profile, otherwise one has to compromise between homogeneity requirements and turbulence levels. The centerline velocity is a reasonably good indicator of the shape of the mean velocity profile. By comparison with more traditional approaches to turbulence generation [9,36], we managed to increase the turbulent Reynolds number dramatically, which was one of the design objectives of the nozzle. In that way, one may reproduce conditions typical of practical system in relatively small experimental systems well-suited for bench-top experiments and computational modeling.

3.2. Turbulence characteristics of selected non-circular jet plates (NCJ)

Data for the NCJ plates are presented in Figs. 11–13. The normalized mean velocity at the centerline (Fig. 11, top left) decreases with H/D_p for all the plates. The central-jet CJ type shows the highest value of centerline velocity, reaching almost twice its average value and being about 30% higher than the other plates at the same position, indicating a highly non-uniform profile, probably caused by the persistence of the high velocity central-jet. The central wake

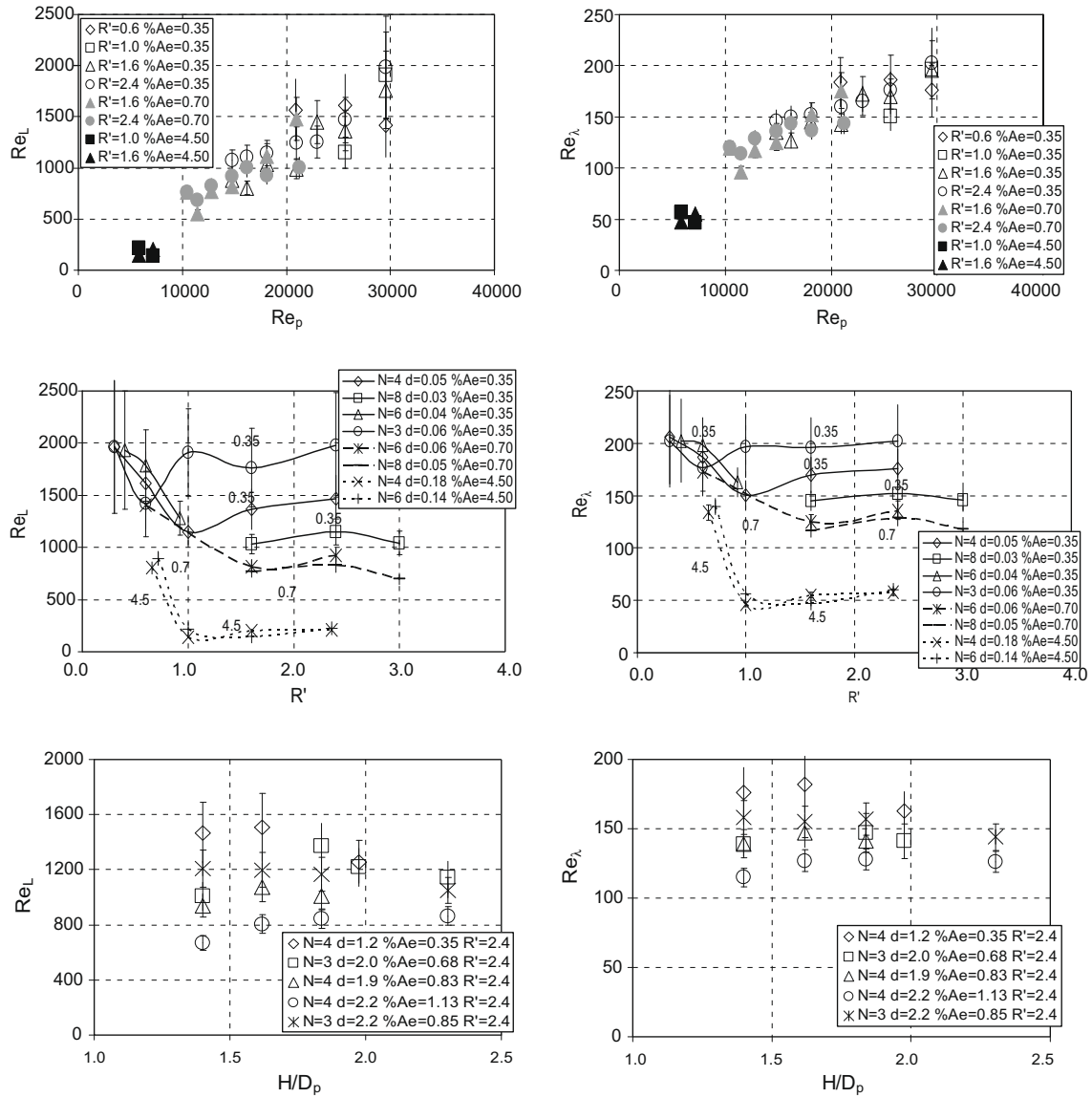


Fig. 9. Turbulent Re numbers of multiple circular jet plates (MCJ Series) based on the integral scale (left column) and the Taylor length scale (right column) at $Re \sim 10,000$ and $H/D_p \sim 1.4$. Top row: as a function of Re_p and parametric in R' and $\%A_e$. Middle row: as function of R' and parametric in N (or d) and $\%A_e$. Bottom row: as function of H/D_p and parametric in N (or d) and $\%A_e$.

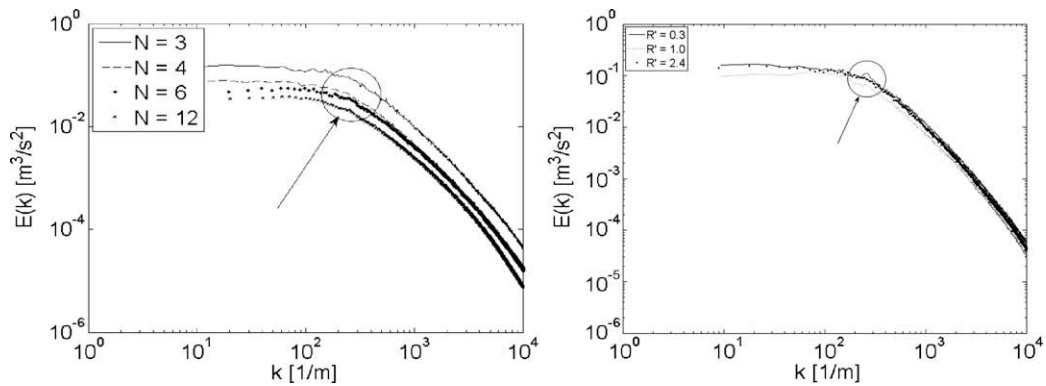


Fig. 10. Energy spectra vs. wavenumber of multiple circular jet plates (MCJ Series). Left: parametric in N . Right: parametric in R' .

(CW) and multi-jet (MJ) plates produce more uniform profiles, in spite of their lower $\%A_e$, probably as a consequence of the hole po-

sition. The turbulence intensity (Fig. 11, top right) decreases with H , and the single-jet (SJ), CJ and CW plates show the highest values,

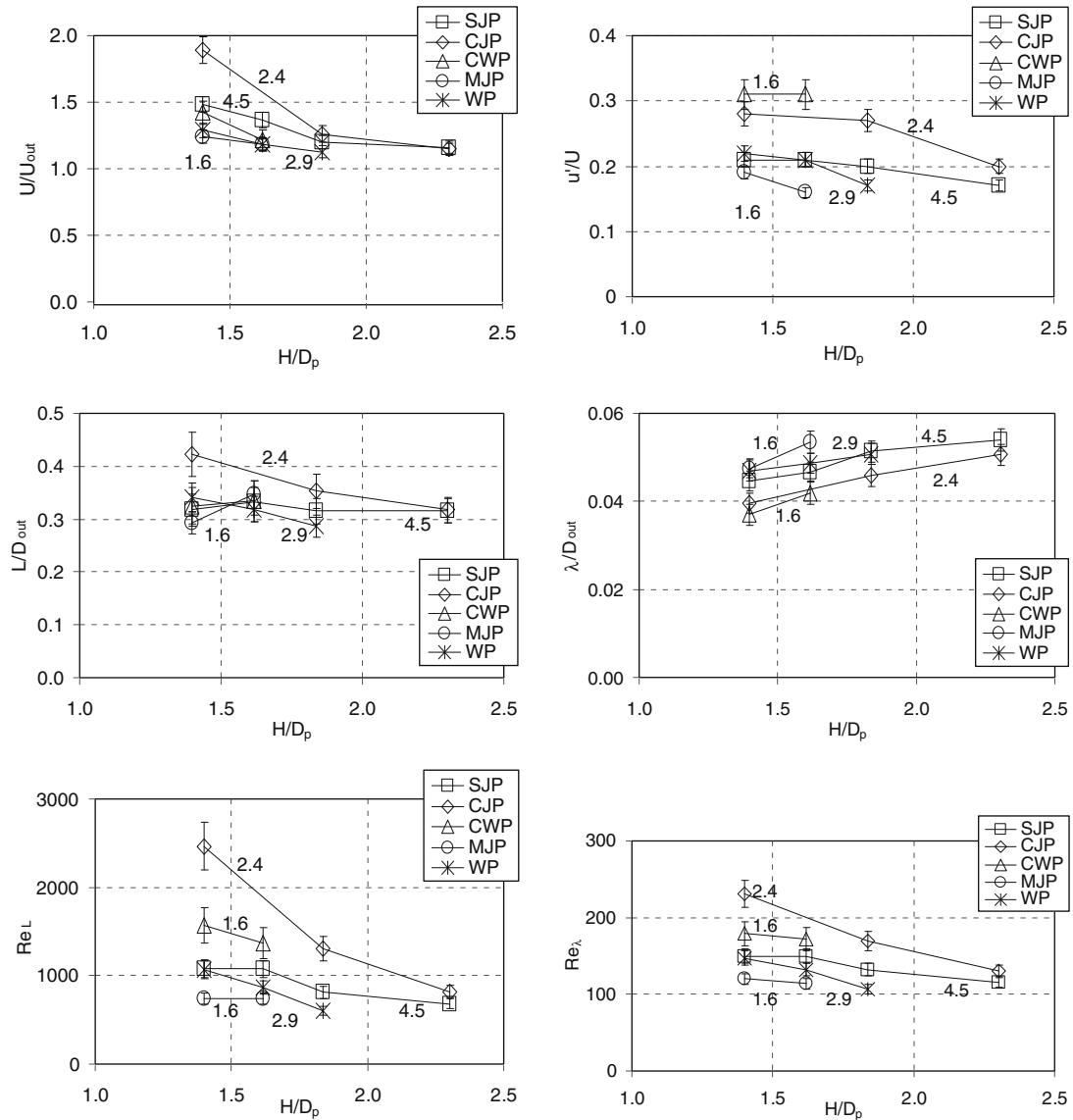


Fig. 11. Performance of non-circular plates at $Re_D \sim 10,000$ as a function of non-dimensional plate position, H/D_p : normalized mean centerline velocity (top left); relative turbulence intensity (top right); normalized integral (center left) and Taylor (center right) length scales; integral (bottom left) and Taylor (bottom right) length scale based Reynolds numbers.

above 20%, in the whole range of H . For these plates, the decrease in the open area has the expected effect of increasing the relative intensity, in agreement with the results from the other families of plates. The CW and MJ series, with the same open area show a significantly different level of turbulence intensity, suggesting that the holes position is also an important parameter. The integral scale (Fig. 11, center left) is relatively constant with H for all the plates and on the order of $0.3D_{out}$, with the exception of the central-jet type, which decreases from about $\sim 0.42D_{out}$ to the common value of $\sim 0.3D_{out}$, in good agreement with the other series. The Taylor scale (Fig. 11, center right) increases for all the plates because of the lower turbulence levels. The turbulent Re numbers (Fig. 11, bottom left) decrease with H for all the plates, following the decrease of the turbulence intensity. The turbulent Re based on the integral scale (Fig. 11, bottom right) shows very high values, on the order of 2500, for the CJ type, because of the larger value of the integral scale at the corresponding positions. The very large values of the integral scale and the corresponding turbulent Reynolds number for the CJ type could be related to a “bump” in the low frequency energy distribution, as shown in Fig. 12 (left). This

bump could indicate some large scale dynamics, which tends to disappear as the plate is moved further away from the nozzle exit section. For every plate, one can define an optimal position, H_{opt} , which maximizes turbulence while maintaining the uniformity and compare the corresponding power spectrum (Fig. 12, right) and radial uniformity (Fig. 13) of the different plates. The energy distribution in the medium frequency range is almost indistinguishable for all the plates. In the low frequency range, the MJ is almost flat, while the others show a more or less pronounced large scale dynamics. The radial profiles of mean velocity (Fig. 13, left) show excellent uniformity for the CJ and SJ types, and reasonably good, to within 8%, for the MJ type. The radial profile of turbulence intensity (Fig. 13, right) is, for all intents and purposes, flat. The small dip at the centerline of the MJ plate could be indicating some incomplete merging of the individual jets.

In summary, among the NCJ plates, the CJ type seem to perform better than the others, in terms of radial uniformity and turbulence levels, even though its open area ratio ($\sim 2.4\%$) is not the smallest, suggesting that the shape is a relevant parameter. In fact, the MJ plate with an open area ratio of $\sim 1.6\%$ behaves quite differently

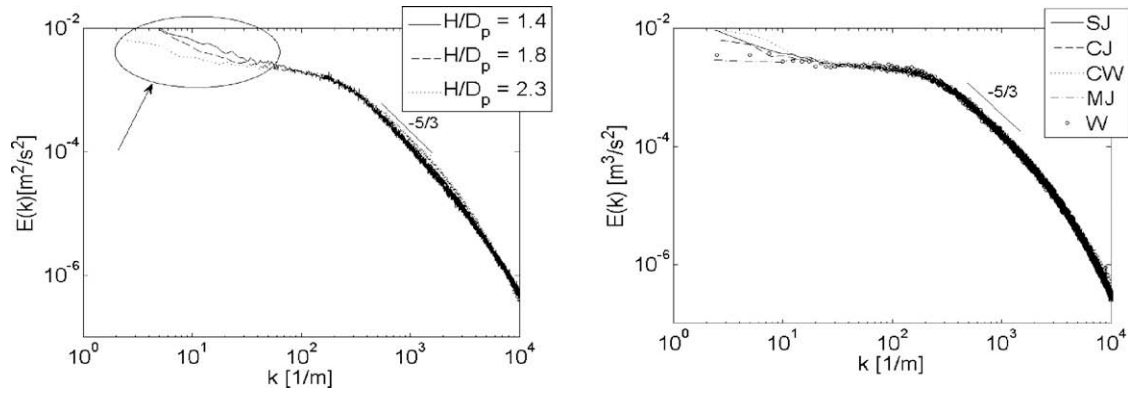


Fig. 12. Energy spectra of non-circular plates versus frequency. Left plot: non-circular central-jet at different distances from the nozzle exit section. Dotted line: $H/D_p \sim 1.4$; dashed line: $H/D_p \sim 1.8$; plain line: $H/D_p \sim 2.3$. Right plot: non-circular plates at their respective optimal position H . Plain line: single-jet plate at $H/D_p \sim 1.8$; dashed line: central-jet plate at $H/D_p \sim 2.3$; dotted line: central wake plate at $H/D_p \sim 1.6$; dashed-dotted line: multi-jet plate at $H/D_p \sim 1.4$; plain line with empty circles: wake plate at $H/D_p \sim 1.6$.

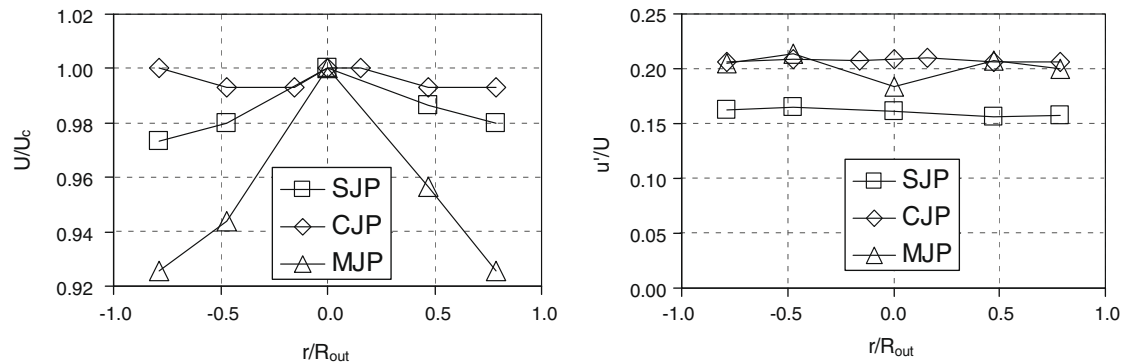


Fig. 13. Non-circular plate radial profiles of mean axial velocity component (right) and the rms axial velocity component (left), scaled respectively by the mean centerline velocity and local mean velocity. Diamonds: single jet plate at $H/D_p \sim 1.8$; squares: central-jet plate at $H/D_p \sim 2.3$; triangles: multi-jet plate at $H/D_p \sim 1.4$.

from the CW plate with the same open area ratio. Overall, the NCJ series achieves larger turbulent Re with a lower blockage than in the MCJ series discussed in Section 3.1, coupled to excellent flow homogeneity. The lack of frequency peaks as found occasionally in the previous series suggests that the holes geometry has also a pronounced effect on the fluid dynamics instabilities and it is a viable way to offset them, if not overcome them. The geometric shape is a powerful parameter offering considerable flexibility.

4. Conclusions

The typical objective of experimental systems for turbulence generation is that of maximizing the turbulent Reynolds numbers to mimic flows of practical interest within the confines of a bench-top experimental system. A systematic experimental study was conducted on a system consisting of a high-blockage plate placed upstream of a contoured contraction. The effect of the geometric parameters of two families of high-blockage plates on the resulting turbulent flow field was systematically studied: one series of plates was characterized by the number and distribution of circular openings; a second one had non-circular opening(s) with different shapes, distribution and position of opening(s). The near field at the centerline of the turbulent free jet at the outlet of the system was characterized by hot-wire anemometry in terms of mean axial velocity, turbulence intensity, turbulence length scales and corresponding Reynolds numbers. The multi circular jet series perform well in terms of achieving higher turbulent levels at a gi-

ven flow rate and preserving radial uniformity, although a spurious peak in the power spectrum in some cases could limit the range of applicability of such plates. In fact, our results suggest that low average velocity with the circular openings at any radial position or high average velocity with the circular openings at large radial positions are required for the peaks to disappear. The non-circular jet series, and specifically the plate with a central-jet, shows the most promising results, with very high turbulence levels and excellent radial uniformity, in both average velocity and turbulence intensity. The analysis of the power spectrum of the flow generated by these plates shows some low frequency dynamics, which may affect some of the results in terms of integral length scales and the corresponding Reynolds number. This effect, though, tends to disappear with increasing distance of the plate from the nozzle exit section. As expected, for all the plates, the turbulence levels decrease with the distance between the plate and the nozzle exit section. In general, the turbulence generation system is flexible, by allowing for independent change of the turbulent Reynolds numbers and of the flow rate, through changes in simple geometrical parameters of the perforated plates. Turbulence generation through high-blockage perforated plates placed upstream a contraction is a viable way to generate intense turbulent fields, as long as precautions are taken to avoid possible instabilities generated by the plate opening(s), shape and position. This new turbulence generation scheme was recently applied to counterflow flames [37] and catapulted them into regimes of relevance to practical systems, well beyond the quasi-laminar conditions that have been studied to date.

Acknowledgments

The support of DARPA under Grant No. DAAD19-01-1-0664 (Dr. Richard J. Paur, Contract Monitor) is gratefully acknowledged. We are indebted to Nick Bernardo for technical assistance in the construction of the hardware and to Dr. Kailasnath Purushothaman for technical discussions.

References

- [1] K.A. Thole, D.G. Bogard, J.L. Whantong, Generating high freestream turbulence levels, *Experiments in Fluids* 17 (1994) 375–380.
- [2] U. Shavit, N. Chigier, Development and evaluation of a new turbulence generator for atomization research, *Experiments in Fluids* 20 (1996) 291–301.
- [3] P.K. Maciejewski, R.J. Moffat, Heat-transfer with very high free-stream turbulence. 1. Experimental-data, *Journal of Heat Transfer – Transactions of the ASME* 114 (1992) 827–833.
- [4] L. Muniz, M.G. Mungal, Effects of heat release and buoyancy on flow structure and entrainment in turbulent nonpremixed flames, *Combustion and Flame* 126 (2001) 1402–1420.
- [5] D. Queiros-Conde, C. Vassilicos, Turbulent wakes of 3-D fractal grids, in: J.C. Vassilicos (Ed.), *Intermittency in Turbulent Flows and other Dynamical Systems*, Cambridge University Press, 2000.
- [6] D. Hurst, J.C. Vassilicos, Scalings and decay of fractal-generated turbulence, *Physics of Fluids* 19 (2007).
- [7] S.H. Kim, H. Pitsch, Mixing characteristics and structure of a turbulent jet diffusion flame stabilized on a bluff-body, *Physics of Fluids* 18 (2006).
- [8] R.K. Cheng, I.G. Shepherd, B. Bedat, L. Talbot, Premixed turbulent flame structures in moderate and intense isotropic turbulence, *Combustion Science and Technology* 174 (2002) 29–59.
- [9] L.W. Kostiuik, K.N.C. Bray, R.K. Cheng, Experimental-study of premixed turbulent combustion in opposed streams. 1. Nonreacting flow field, *Combustion and Flame* 92 (1993) 377–395.
- [10] A. Kitajima, T. Ueda, A. Matsuo, M. Mizomoto, A comprehensive examination of the structure and extinction of turbulent nonpremixed flames formed in a counterflow, *Combustion and Flame* 121 (2000) 301–311.
- [11] A. Yoshida, T. Igarashi, Y. Kotani, Extinction of turbulent diffusion flames by Kolmogorov microscale turbulence, *Combustion and Flame* 109 (1997) 669–681.
- [12] A. Yoshida, An opposed jet burner for the study of high-intensity combustion, *Measurement Science and Technology* 10 (1999) N149–N151.
- [13] D. Geyer, A. Kempf, A. Dreizler, J. Janicka, Scalar dissipation rates in isothermal and reactive turbulent opposed-jets: 1-D-Raman/Rayleigh experiments supported by LES, *Proceedings of the Combustion Institute* 30 (2005) 681–689.
- [14] D. Geyer, A. Dreizler, J. Janicka, A.D. Permana, J.Y. Chen, Finite-rate chemistry effects in turbulent opposed flows: comparison of Raman/Rayleigh measurements and Monte Carlo PDF simulations, *Proceedings of the Combustion Institute* 30 (2005) 711–718.
- [15] D. Geyer, A. Kempf, A. Dreizler, J. Janicka, Turbulent opposed-jet flames: a critical benchmark experiment for combustion LES, *Combustion and Flame* 143 (2005) 524–548.
- [16] A. Kempf, H. Forkel, J.Y. Chen, A. Sadiki, J. Janicka, Large-eddy simulation of a counterflow configuration with and without combustion, *Proceedings of the Combustion Institute* 28 (2000) 35–40.
- [17] S.R. Turns, *An Introduction to Combustion: Concepts and Applications*, Second ed., McGraw-Hill, Boston, 2000.
- [18] B.D. Videto, D.A. Santavicca, A turbulent-flow system for studying turbulent combustion processes, *Combustion Science and Technology* 76 (1991) 159–164.
- [19] B. Bedat, R.K. Cheng, Experimental-study of premixed flames in intense isotropic turbulence, *Combustion and Flame* 100 (1995) 485–494.
- [20] International Workshop on Measurement and Computation of Turbulent NonPremixed Flames, 2008. <<http://www.ca.sandia.gov/TNF>>.
- [21] A.V. Oppenheim, R.W. Schaffer, *Discrete-Time Signal Processing*, Prentice-Hall, Upper Saddle River, NJ, 1989.
- [22] M.J. Barrett, D.K. Hollingsworth, On the calculation of length scales for turbulent heat transfer correlation, *Journal of Heat Transfer – Transactions of the ASME* 123 (2001) 878–883.
- [23] J.O. Hinze, *Turbulence*, McGraw-Hill, 1975.
- [24] L.H. Benedict, R.D. Gould, Towards better uncertainty estimates for turbulence statistics, *Experiments in Fluids* 22 (1996) 129–136.
- [25] F. Jorgensen, How to Measure Turbulence with Hot-Wire Anemometers (A Practical Guide), Dantec Dynamics, Dantec Dynamics, 2002.
- [26] H.H. Bruun, *Hot-Wire Anemometry: Principles and Signal Analysis*, Oxford University Press, London, 2000.
- [27] E. Villermaux, E.J. Hopfinger, Periodically arranged co-flowing jets, *Journal of Fluid Mechanics* 263 (1994) 63–92.
- [28] T.J. Craft, B.E. Launder, On the spreading mechanism of the three-dimensional turbulent wall jet, *Journal of Fluid Mechanics* 435 (2001) 305–326.
- [29] E. Villermaux, J. Sommeria, Y. Gagne, E.J. Hopfinger, Oscillatory instability and genesis of turbulence behind a high solidity grid, *European Journal of Mechanics B – Fluids* 10 (1991) 427–439.
- [30] E. Villermaux, E.J. Hopfinger, Self-sustained oscillations of a confined jet – a case-study for the nonlinear delayed saturation model, *Physica D* 72 (1994) 230–243.
- [31] P. Legal, I. Peschard, M.P. Chauve, Y. Takeda, Collective behavior of wakes downstream a row of cylinders, *Physics of Fluids* 8 (1996) 2097–2106.
- [32] B.C. Khoo, T.C. Chew, P.S. Heng, H.K. Kong, Turbulence characterization of a confined jet using PIV, *Experiments in Fluids* 13 (1992) 350–356.
- [33] J.S. Brown, B.C. Khoo, A.A. Sonin, Rate correlation for condensation of pure vapor on turbulent, subcooled liquid, *International Journal of Heat and Mass Transfer* 33 (1990) 2001–2018.
- [34] A.A. Sonin, M.A. Shimko, J.H. Chun, Vapor condensation onto a turbulent liquid. 1. The steady condensation rate as a function of liquid-side turbulence, *International Journal of Heat and Mass Transfer* 29 (1986) 1319–1332.
- [35] K. Sardi, A.M.K.P. Taylor, J.H. Whitelaw, Extinction of turbulent counterflow flames under periodic strain, *Combustion and Flame* 120 (2000) 265–284.
- [36] E. Korusoy, J.H. Whitelaw, Extinction and relight in opposed flames, *Experiments in Fluids* 33 (2002) 75–89.
- [37] G. Coppola et al., Highly Turbulent Counterflow Flames: A Laboratory Scale Benchmark for Practical Systems, *Combustion and Flame* (2009), doi:10.1016/j.combustflame.2009.03.017.